Identification of River Ice Types on the Peace River using RADARSAT-1 SAR Imagery

Frank Weber and Dan Nixon
BC Hydro
6911 Southpoint Drive, Burnaby, BC, Canada, V3N 4X8
Frank.Weber@BCHydro.bc.ca and Dan.Nixon@BCHydro.bc.ca

Jeff Hurley
RADARSAT International
13800 Commerce Parkway, MacDonald Dettwiler Building, Richmond, BC, Canada, V6V 2J3
JHurley@RSI.ca

Abstract
The winter regime of the Peace River in northern British Columbia and Alberta is a determining factor for the operation of BC Hydro's Williston Reservoir. Therefore, several Fine Beam RADARSAT-1 SAR satellite images were acquired in winter / spring 2000 and 2001, and analyzed for ice types and ice-front locations. Video footage of the ice conditions on the Peace River was obtained from aerial ice observations that were conducted simultaneously with the image acquisitions. The analysis of the images was done 1) visually and 2) using an Unsupervised Fuzzy K-means Classification. By visually analyzing the images, several river ice features could be identified, including frazil pans, frazil floes, shore ice composed of frazil slush, melting ice, and brash. Juxtaposed and secondary consolidated ice could be distinguished relative from each other. Under most conditions encountered in this study, the location of the ice front coincided with the head of the complete ice cover, and was, therefore, discernible from the SAR images. Ambiguities arose from open water and freeze-over border ice. By comparison, the Unsupervised Classification broke the data into four classes, which represent river signatures ranging from open water to ice with a strong radar return. No physically existing ice types could be assigned to the three categories representing ice features. However, the spatial distribution of ice features closely matches the visible ice types on the river. User interpretation is required to derive ice types from the classification maps. This study suggests that the visual analysis of SAR imagery is very powerful for river ice type classifications, but that more effort needs to be made to further develop automated river ice classification techniques.

1. Introduction

In cold climates, the winter regime of rivers and lakes is often a determining factor in the management of water resources. This is particularly true for northern rivers, which freeze up in an upstream direction. For example, the knowledge of the ice formation, ice types, and ice strength is necessary for the operation of hydropower generating facilities.

The Peace River System

The Peace River originates in northeastern British Columbia, Canada, west of the Rocky Mountains at the confluence of the Parsnip and Finlay Rivers (Figure 1). Through a gap in the Continental Divide, the Peace River then flows in an easterly direction for approximately 390 kilometers to the Town of Peace River (TPR). Here the Peace River changes its course to a northerly and later northeasterly direction for approximately 850 kilometers. At the confluence with the Rivere des Rochers it forms the Slave River (Assaf et al., 1995).

In 1972, the construction of the British Columbia Hydro and Power Authority's (BC Hydro) Bennett Dam was completed. The dam created the Williston Reservoir, which is BC Hydro's largest reservoir. Since then, the hydraulic profile of the Peace River has been dramatically altered. The winter flows in the Peace River have increased while the spring freshet was significantly attenuated. Because the Peace River is a north flowing river the freeze-up starts early in the year many miles to the north. As the winter progresses southward, the ice cover on the river moves upstream past the TPR. Ice jam flooding at the TPR has historically occurred in pre-regulation. These events were usually a result of the onset of the freshet lifting the ice cover.

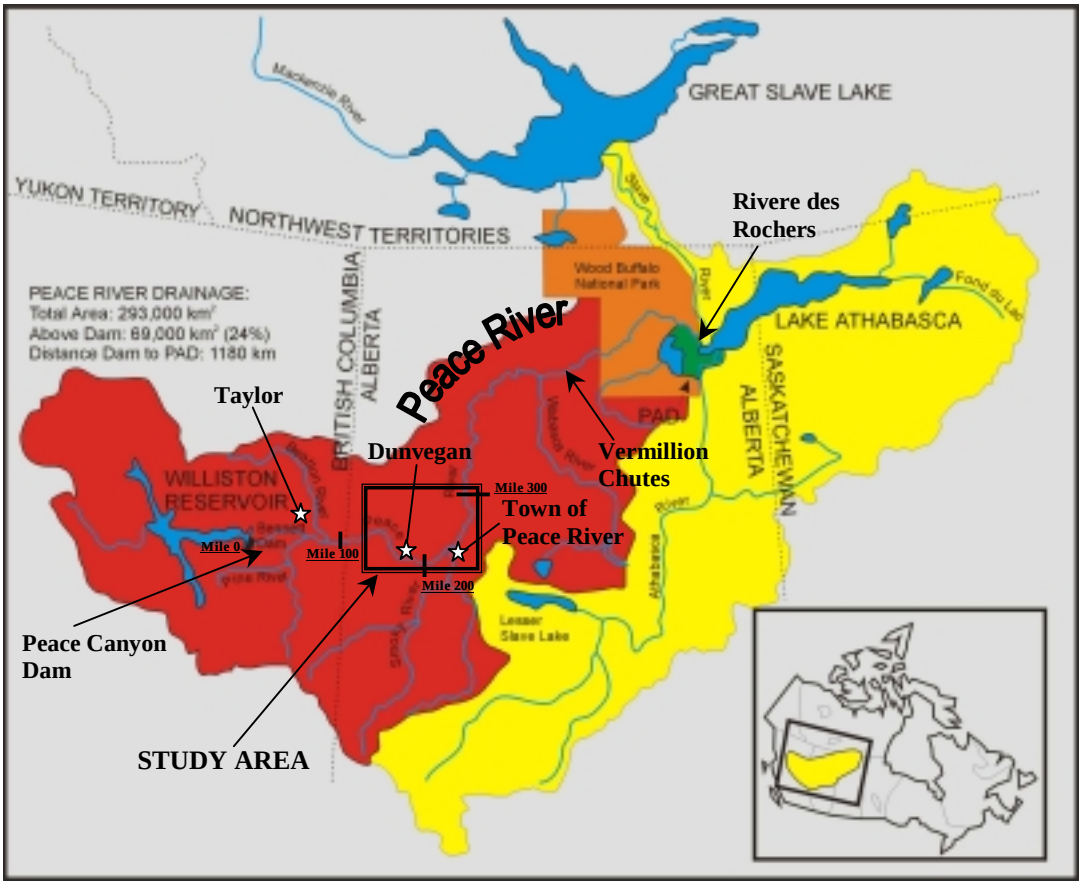

Figure 1: Overview map of the Peace River

In 1973 and 1974 the operation of the Bennett Dam was thought to have precipitated the ice jam events at the town. The Alberta / BC Joint Task Force on Peace River Ice (Task Force) was formed in 1974, in response to these events, with a mandate to study and control the break-up processes. The mandate was expanded to include freeze-up processes after the ice jam events in 1979 and 1982 again caused flooding in the town. The Task Force developed operating guidelines designed to maintain a relatively steady release from the reservoir during the freeze-up period through the TPR reach such that the freeze-up levels at town were kept low. The low freeze-up levels would ensure sufficient freeboard to keep an ice-jam event from overtopping the dykes. When the ice front is within three days of Mile 255 (10 miles downstream of the TPR) the flows from Peace Canyon Dam are reduced to a pre-determined discharge (Note: the river mileage reference point is Bennett Dam at Mile 0). This reduced flow will meet the advancing cover at Mile 255 and is held steady until the ice cover has moved upstream of Dunvegan (Mile 185). Once the ice cover is deemed to be competent to resist increased flows, BC Hydro is cleared to increase discharges (Trillium Engineering and Hydrographics Inc. et al., 1996).

Ice monitoring

BC Hydro's decision whether the ice is strong enough to resist secondary consolidation is currently based on information collected by an ice-monitoring program that includes observers periodically performing aerial surveillance of the river. The uncertainty of the duration of the steady-flow release influences power production and BC Hydro's flexibility to meet their domestic load.

Extensive ice monitoring on the Peace River started in 1982. Observation flights start in late November after the ice front has traveled upstream of Vermilion Chutes (Mile 500) and continues throughout the winter and spring until the ice front has passed downstream of Mile 500 again. Aerial ice surveillance flights are conducted on a weekly to bi-weekly basis once the ice front is upstream of Mile 430. Additionally, the local residents living along the Peace River provide information when the ice front has moved past their farms. As the ice front approaches the TPR the rate of advance is closely watched.

The responsibility for ice observations is transferred from Alberta Environment to BC Hydro when the ice front is upstream of Dunvegan. Information from ground and aerial surveys is reported to the Task Force and the TPR. The information provided is used for reservoir management and provides an archive of ice front locations and ice conditions.

Since the launch of satellites that operate in the visible, near-infrared, thermal, and microwave spectrum, satellite imagery can potentially be used for ice observations. Due to its night-and-day, and all-weather viewing capabilities, the Synthetic Aperture Radar (SAR) satellite RADARSAT-1 was chosen for this study. However, the capability of RADARSAT-1 satellite image as a means to monitor freshwater ice processes on a spatial and temporal basis still has to be proven. This study evaluates the options and limitations of the use of RADARSAT-1 C-band SAR images to identify river ice types. In particular, the potential to monitor ice features that indicate the stability of the river ice cover, such as juxtaposed ice, secondary consolidated ice, and open water were investigated. Satellite imagery was analyzed to determine whether the ice front location could be ascertained. In this paper, the results from a visual image analysis and an Unsupervised Classification are discussed and compared to aerial photographs and video footage. The study focuses on the Peace River in the vicinity of the TPR (Figure 1).

River ice types

River ice processes are schematized in Figure 2. Figure 2 also shows the main ice types found on the Peace River. In the Peace River, frazil ice generation is the dominant river ice formation process. The maximum ice thickness is 0.8 meters to 1.2 meters (Trillium Engineering and Hydrographics Inc. et al., 1996).

Under regulated conditions freeze-up occurs on the Peace River by an orderly progression of the ice cover from the Slave River to the Town of Taylor. The ice cover progresses upstream by a combination of juxtaposition and consolidation. At the TPR an ice cover typically forms between late-December and mid-January. However, it has formed as early as early-December as in 1985 and as late as mid-February as in 1993 and 2001. Break-up normally occurs at the TPR in April. Break-up has been observed as early as mid-March as in 1993 and as late as early-May as in 1979. A mechanical break-up at the TPR can be triggered by an intensive snowmelt event in the Smoky River basin when a dynamic run on the Smoky River meets the intact ice cover on the Peace River just upstream of the TPR (Trillium Engineering and Hydrographics Inc. et al., 1996).

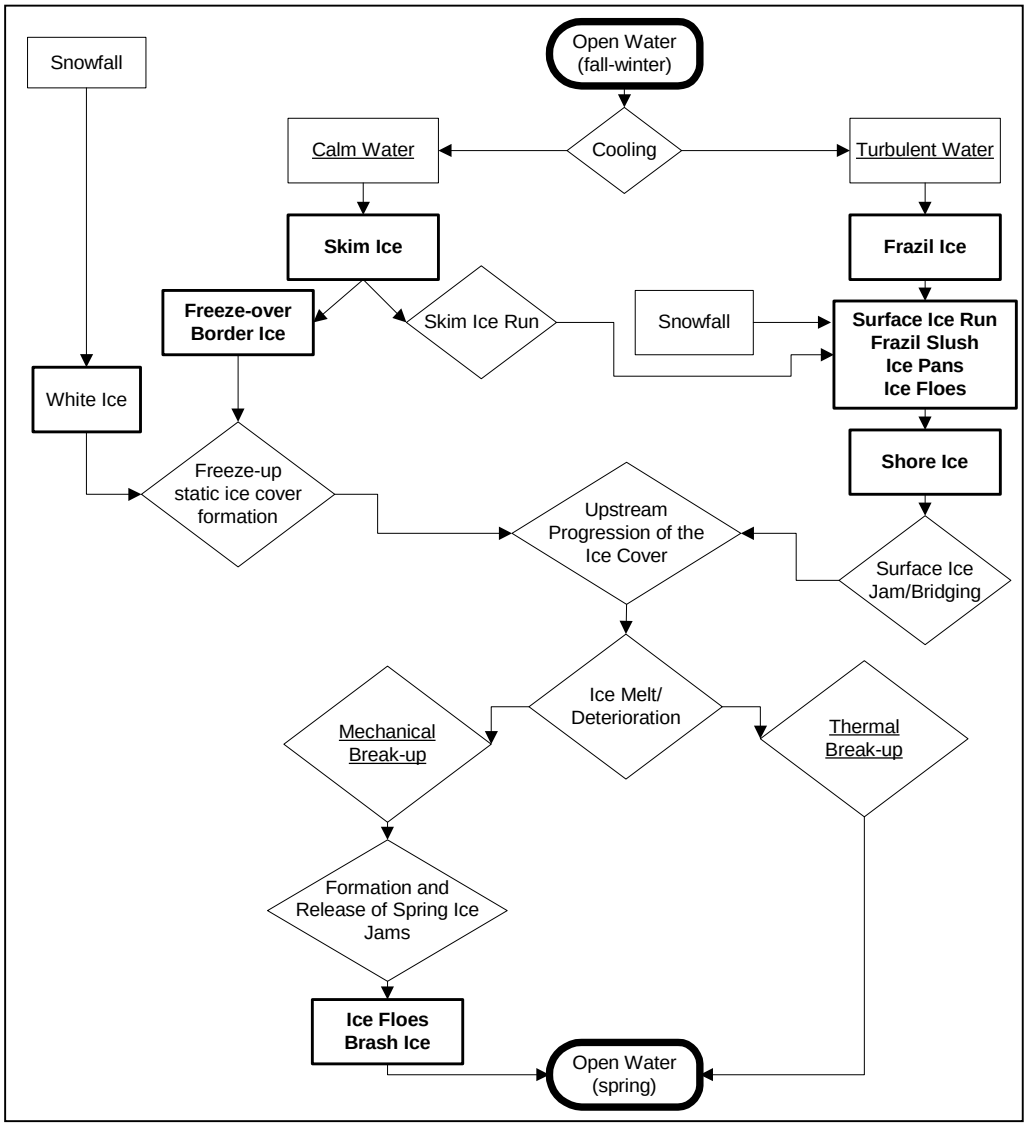

Figure 2: River ice processes adapted from Shen 1996

2. Radar Remote Sensing

Radar data are difficult to interpret, because the microwave signal is able to penetrate a target and thus provides information on the surface and the internal structure of the material (Hall, 1998). Active microwave instruments record the backscattered radar signal, which is composed of contributions from surface and volume scattering. In general, the strength of the backscattered signal depends on the material's dielectric constant, surface roughness, and incident angle of the incoming radiation (Raney, 1998).

Dielectric properties

The dielectric properties of a material are characterized by its dielectric constant. The dielectric constant is also known as the complex permittivity and describes the electrical properties of a material. The most important dielectric constants for the analysis of freshwater ice are summarized in Table 1.

Table 1: Dielectric constants

	Dielectric constant	Source
Air	1	
Freshwater ice – clear ice with air bubbles > 0.6	2.99	Cooper et al. (1976)
Freshwater ice – milky ice	3.08	Cooper et al. (1976)
Freshwater ice – clear ice	3.17	Evans (1965)
Dry snow	1.2-2.0	Hallikainen and Ulaby (1986)
Wet snow	>35	Hall (1998)
Water	81	

The dielectric properties of a material determine the electromagnetic loss caused by absorption. If the absorption loss is low, the penetration depth of the microwave signal is high. A low dielectric constant implies low moisture content and low signal return. For example, freshwater ice is a low-loss medium. The potential penetration depth into freshwater ice ranges from 100 meters to 10 meters at 1 GHz and 10 GHz, respectively (Hallikainen & Winebrenner, 1992). As a result of the high penetration depth of microwaves into freshwater ice, the backscatter coefficient is not limited to the response of the uppermost ice layers.

In contrast, when the dielectric constant of the imaged material is large, then the absorption loss is high and the penetration depth is low. For example, liquid water is a high-loss medium. When the moisture content in snow or ice is high, then the penetration depth is reduced to the uppermost centimeters or to a depth of approximately one wavelength. Approximately 3 vol-% moisture causes a significant reduction of radar penetration. Wet snow with 3 vol-% water content reduces the penetration depth to 10 centimeters at 5 Ghz (Hallikainen & Winebrenner, 1992). Similarly, the appearance of a given ice feature differs significantly in wet versus dry conditions. When ice is covered by water, its brightness differs from that encountered in dry conditions.

Surface roughness: surface scattering and specular reflection

Diffuse scattering and specular reflections occur at interfaces between materials of significantly different dielectric properties. These interfaces are not necessarily the optically observed physical surfaces. For example, if freshwater ice is underlain by water, the microwaves are predominantly scattered from the ice/water interface and only to a minor extent by the air/ice interface (Elachi et al. 1976). The dielectric discontinuity of the ice/water interface is 3.2/81, whereas the ice/air discontinuity is only 3.2/1. In this case, the bottom surface of the ice is imaged.

Whether a material appears smooth or rough depends on the length of the electromagnetic wave and the incident angle. In the case of RADARSAT-1 remote sensing (lambda is 5.6 centimeters), surfaces with discrete surface height elements higher than approximately 0.56 centimeters appear rough. Smooth surfaces reflect the impinging energy away from the surface, with the angle of reflection being equal to the angle of incidence. Only if the smooth surface is perpendicular to the incident energy, then the energy returned to the antenna is intense. In contrast, radiation is scattered diffusely from rough surfaces. Typically, increasing roughness leads to increasing brightness of the radar backscatter. For example, a smooth water surface, smooth black ice, or smooth, wet snow surface reflect the incident energy specularly in only one direction. As a result, the backscatter is low (Bryan & Larson, 1975). In the case of wet snow, the surface roughness has a great impact on the backscattered signal. If a wet snow surface is rough because of rain rills or trees, the backscatter from this surface is high due to corner reflection. Very rough ice, such as heavily consolidated ice, has high radar returns (Bryan and Larson, 1975).

Volume scattering

Volume scattering is the process by which a radar signal is not only reflected by the surface, but it is also scattered by dielectric discontinuities within a host medium. Volume scattering depends on the heterogeneous nature of the imaged object (Raney, 1998). The part of the backscatter resulting from volume scattering is influenced by the size of the scatterer within the medium. For example, freshwater ice and snow are heterogeneous substances. They are mixtures of ice crystals, liquid water, air, and impurities. Additionally, cracks may occur in freshwater ice. The microwave energy can be scattered from these mixture constituents (Drinkwater, 1989). If, for example, elongated bubbles with an adequate size relative to the radar wavelength are present in ice, then radar returns from ice are relatively high (Morris et al., 1995).

In contrast, if the size of the scatterer is small relative to the wavelength, the volume scattering component of the microwave return is low. For example, the snow crystal size typically encountered in the field (i.e. 0.05–3 millimeters) is too small to cause significant volume scattering. Therefore, C-band radar signals penetrate dry snow almost unaffectedly. In shallow snowpacks, the signal returned stems predominantly from the underlying ground. In contrast, in thick dry snowpacks, such as dry polar snowpacks on glaciers, the backscatter is entirely caused by volume scattering. However, the magnitude of the backscatter is relatively low (Rau et al., 2000).

Incident angle

The incident angle influences the roughness sensitivity of the imaging sensor and, therefore, the backscatter and image tone. The local incident angle is defined “as the angle between the radar line-of-sight to the point in question, and the normal to the tangent plane at that point” (Raney, 1998:36). In a single image, the average incident angle (angle between the radar line-of-sight to the point in question, and the vertical at that point) increases from the near range to the far range, when the terrain slope is constant. In this study, the effects of the terrain slope can be neglected, because only the river plane is analyzed. In theory, ice features in the river plane are brighter in the near range than in the far range. For the same reasons as described above, images taken in the near range are theoretically brighter than images, taken in the far range.

In summary, the backscatter received by the SAR antenna can be as complex as the sum of surface scattering at the air/snow, snow/ice, ice/water, ice/ground interfaces, and volume scattering within the snowpack and ice layers.

3. Methods

Field observations

In this study, ice information was obtained from regular and special aerial ice observations. The ice observations from regular aerial surveys include the documentation of weather conditions, the ice front location, and the river ice conditions. The river ice documentation includes the occurrence and location of certain ice types, the percentage ice coverage, size and location of open-water leads, water on ice, and occasionally information on the flow conditions and backwater flooding upstream of the ice front. During special observation flights, which were scheduled to be simultaneous with RADARSAT-1 image acquisitions, the river ice was filmed with a hand-held video camera and photographed with a still camera.

RADARSAT-1 data

RADARSAT-1 SAR data were used for the study of freshwater ice types. RADARSAT-1 operates in a sun-synchronous, dawn-dusk orbit. The local overpass time is approximately 7 a.m. and 7 p.m. MST for descending and ascending orbit, respectively. The sensor transmits and receives horizontally polarized microwaves (HH) at 5.3 GHz frequency. This corresponds to a wavelength of 5.6 centimeters. Table 2 summarizes the RADARSAT-1 images analyzed. All images used in this study were taken in the Fine Beam mode with area coverage of 50 kilometers x 50 kilometers and a ground resolution of approximately 8 meters (RSI, 1999). Due to the small spatial extent of RADARSAT-1 Fine Beam images, the effects of the incident angle on the backscatter in the near and far range are presumably small. Image acquisition was scheduled so that the ice front was located in the image. For this reason the beam mode was not kept constant, but ranged from Fine-1-Near (F1N) to Fine-5-Far (F5F). Consequently, the average incident angle ranged from 37 degrees to 48 degrees. Image signal data were processed by RSI to a path-oriented data product in which the scenes are aligned parallel to the satellite's orbit path.

Table 2: Images analyzed

Acquisition Date/MST	Beam Mode	Orbit	Visual Analysis	Unsupervised Classification
January 28, 2000 18:41	F1F	Ascending		✓
February 3, 2000 7:11	F1F	Descending		✓
February 10, 2000 7:07	F3N	Descending	✓	✓
March 29, 2000 7:06	F1F	Descending	✓	
April 5, 2000 7:02	F2F	Descending	✓	
January 25, 2001 6:58	F4N	Descending	✓	
February 25, 2001 18:49	F5F	Ascending	✓	
March 7, 2001 7:02	F3F	Descending	✓	

Image processing

Further processing of the path-oriented image data was done differently for the visual analysis and Unsupervised Classification due to the availability of different software packages for both project partners (BC Hydro and RSI). The visual analysis was performed at BC Hydro using the IDRISI32 software. The images were enhanced using linear stretching, and the gaussian or median filter with a 3x3 kernel size. Subsequently, the path-oriented, visually enhanced images were re-sampled to the UTM grid.

For the Unsupervised Classification, image analysis was carried out at RSI using the PCI EASI/PACE software. Emphasis was placed on developing a methodology that could be reproduced in an operational environment. Such an environment requires a system of rapid image processing and minimal user intervention. The input product to the processing chain in each case was a RADARSAT-1 CEOS format image, with Path Image (SGF) processing.

The initial step, as with most commercial packages, is the ingest of the CEOS data into the proprietary format of the software. With PCI, this creates a 16-bit unsigned raster image that contains georeferencing information, but is not map oriented. Extracted from the CEOS ancillary data are the latitude and longitude for 256 points evenly distributed throughout the image. These reference points are used in a latter step to geocode the imagery.

The utilization of single-look Fine Beam imagery, while providing the highest resolution, is characterized by a high amount of speckle. To remove or reduce this high frequency noise, specific SAR filters were used. The best filter uses an adaptive approach that smoothes the image data without removing edges, thin linear features or point targets. Qualitative visual analysis of several different filters was carried out. The best results were derived using the Kuan SAR filter with a 5x5 kernel size. It should be noted that the filtering step can potentially be performed under a graphic mask. The benefit of this is to greatly reduce the processing time. Actual process flow could be altered in an operational system, such that the imagery would be geocoded before filtering to make use of an existing river mask. Should this route be adopted it must be understood that the geocoded imagery would contain altered Digital Numbers due to the resampling algorithm. If the methodology developed does not rely on purely quantitative analysis then this fact becomes less of an issue.

To reduce data volume and the computing time for the various processes, the imagery was scaled from 16 to 8 bits. This effectively reduces an image by 50% (e.g. from 120Mb to 60Mb). An intelligent scaling approach was adopted, whereby an analysis of the 16 bit data histogram was performed. Mean and standard deviation values were noted and used in the scaling process. As every scene results in a unique histogram, 100% repeatability of the scaling parameters proves difficult. However, by controlling the inputs to the scaling process, it is possible to produce qualitatively similar 8 bit products from temporally diverse imagery. The scaling procedure also effectively acts as an enhancement. The data, which typically appears dark in its original form, will be brighter and visually more acceptable after the scaling.

The geocoding procedure transforms the imagery into a map projection system. For this project, imagery was either projected based on the orbital ephemeris data or tied to an image that was previously geocoded. In this case, three of the scenes were collected over virtually the same area. One image was chosen as the master and geocoded using the ephemeris data. This typically provides horizontal accuracy better than 100 meters (at sea level). The other two scenes were subsequently geocoded using the master image. Approximately 20 tie points were utilized to provide adequate matching. As imagery from opposite look directions was collected, inherent SAR distortions made accurate image matching quite difficult. To overcome this it was necessary to focus the tie points along the course of the river. This ensured that the matching between images would be highest along the river.

Image analysis

The analysis of the georeferenced and enhanced images was done 1) visually and 2) using an Unsupervised Classification method.

Visual Classification

Visual image analysis utilizes tone, texture, shape, and size to identify target parameters and, hence, ice types. Target parameters used for ice type classification are surface roughness, material structure, shape, size, and dielectric properties. Microscale surface roughness has the greatest impact on tone. Tone is the mean brightness of a distributed feature in an image. Mesoscale roughness characteristics have an influence on texture. Texture describes the variation in tone between individual resolution cells. In addition, the parameters shape and size become important when identifying frazil floes and consolidation lobes.

Unsupervised Classification

The two primary methodologies for classification are Supervised and Unsupervised Classification. Supervised Classification involves three steps, beginning with the identification of training areas by a trained analyst. This is a time consuming and potentially variable process depending on the analyst's skill and experience. Once complete, the training areas are used as a basis for the classification and then a final product is output as a thematic layer.

In an attempt to streamline the process, the focus during this project was on Unsupervised Classification. This approach does not require the time intensive training areas to be created. Rather, natural groupings of pixels are created and interpreted later to determine what each class is. Several variants of this approach were examined in the project, including Isodata, K-means and Fuzzy K-means clustering. The best results were generated using the Fuzzy K-means algorithm. The target number of output classes is selected by the user before running the classification. Ideally, the number of classes will approach the number of classes that the analyst can see in the image. For the river features, it was possible to clearly distinguish between four classes. These ranged from open water to ice features with a large backscatter. The testing of the various unsupervised approaches was centered on creating a thematic map with as close an interpretation as was possible through visual analysis. The availability of excellent ground truth data from near-coincident airborne flights proved invaluable in the analysis of results. A mode filter was used to clean up the results and produce a more uniform thematic representation.

4. Results and Discussion

Visual analysis

Open water, frazil pans, frazil floes, and border ice

Figure 3 shows the Peace River from Mile 146 to 149 on the February 10, 2000 SAR image. The image was taken during freeze-up. The air temperature at the time of image acquisition was approximately –20ºC. This is important to note as the thin dry snow cover, that covered the area, is nearly transparent to SAR signals at this ambient air temperature.

Open water at location A in Figure 3 can be easily identified on the Peace River images, because smooth water surfaces act as specular reflectors from which very low backscatter is returned. If there was wave action on the Peace River, the signal response could potentially increase. However, wind induced waves and turbulent waters are minimized on the Peace River due to an incised valley, which prevents winds from creating waves, and a low hydraulic gradient.

On February 10, the frazil ice production was high. As a result, frazil pans formed. Upstream of the constriction, the concentration of frazil pans (B) increases towards the concave bank. Gray frazil pans are in sharp contrast to the black water, thereby creating mottled-texture areas. The backscatter of frazil pans is probably caused by a moderately rough ice/water interface. Backscattering at air bubbles trapped in the porous ice further increases the signal strength. Andres (1995: 60) describes frazil pans as "a porous mass of frazil, capped by a solid ice crust that results from freezing at the interface between the air and the top of the floe". As a result, surface and volume scattering from frazil pans are relatively strong. Similarly, Leconte & Klassen (1991) concluded that strong returns originate from frozen frazil slush.

Shore ice is indicated in the SAR image with different brightness levels. For example, shore ice at the area near Location C1 produces bright tones and a homogeneous texture. It is speculated that shore ice upstream of the

constriction (C1) is composed of congealed frazil pans, which are not frozen to the bed. As described above, backscatter from frazil pans is relatively high due to surface and volume scattering. In contrast, shore ice at Location C2 is characterized by relatively dark tones. The relatively low backscatter is attributed to ice that is frozen to the streambed. The dielectric constant of sediment is lower than that of water, hereby creating a less significant interface at the bottom of the ice cover than at the ice/water interface. Stronger radar reflections occur at interfaces with greater difference in dielectric constant. Thus, a floating ice cover reflects the radar signal more than ice frozen to the bed (Hall, 1998). This phenomenon can also be observed at Location C3. Here, shore ice covers a low lying gravel bar. Where the ice is frozen to the ground, the backscatter is relatively low. In contrast, the floating part of the ice cover appears bright.

At the constriction (D), frazil pans are compressed. On the downstream side of the constriction, the ice cover disintegrates into frazil floes (E) and pans. Frazil floes can be distinguished from other ice types by their relatively bright tone, relatively large size, and irregular shape.

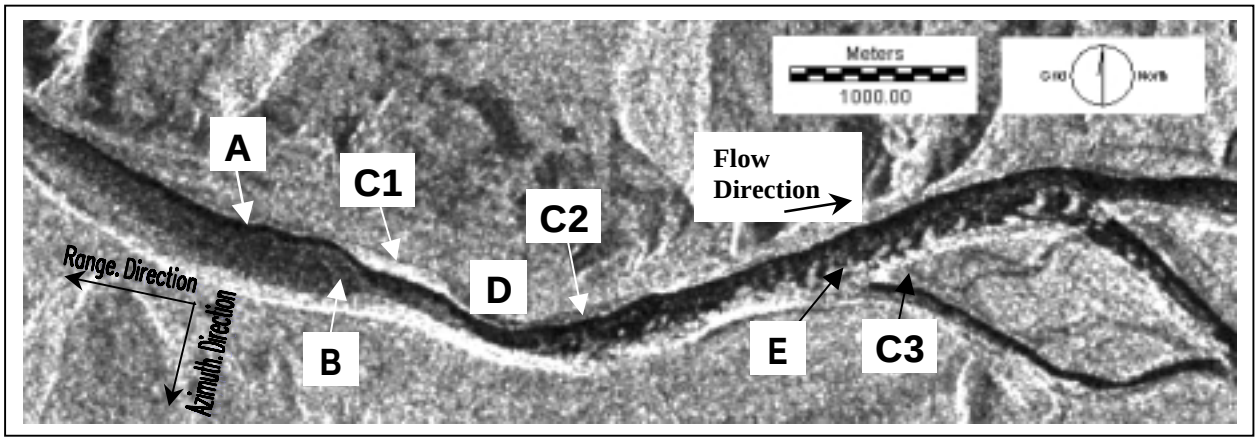

Figure 3: February 10, 2000 RADARSAT-1 image (F3N, descending)

Ice front

On January 25, 2001 at 14:15 p.m. the ice front was located at Mile 253, that is 7 miles downstream of the Highway 2 bridge at TPR. The ice cover was advancing upstream at a rate of 1 mile per day. The air temperature was approximately –10ºC at the time of image acquisition.

Two criteria define the ice front. Firstly, the ice front is the boundary between partial and complete ice coverage. Secondly, the frazil pans and floes must be static. In Figure 4, the head of the complete ice cover can be determined from the SAR image at Location A. Gray frazil pans (B) contrast the black water (C) just upstream of the boundary between partial and complete ice coverage. During the January 25, 2001 observation flight, the head of the complete ice cover was several hundreds of meters upstream of the ice front. Ice between the head of the complete ice cover and the ice front was still mobile due to compression processes. Because of the lack of knowledge of the ice cover dynamics, when interpreting a single SAR image, the exact location of the ice front could not be derived from this SAR image.

Close to the ice front, a juxtaposed ice cover prevails (D). It is characterized by an intermediate gray color. As for frazil pans, a moderately rough ice/water interface, and a coarse ice structure cause the backscatter. From the ice front to the downstream river bend, the ice cover rapidly consolidates.

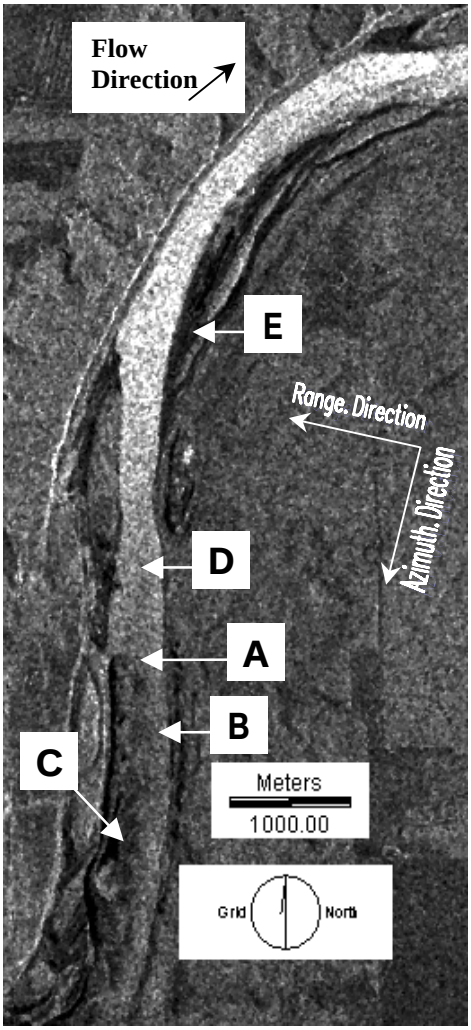

Figure 4: January 25, 2001 RADARSAT-1 image (F4N, descending)

In this image, both freeze-over border ice (E) and open water (C) appear dark. It is understood that freeze-over border ice acts as specular reflector due to a smooth ice/water interface and a compact, bubble-free structure. Photographs had to be used to identify freeze-over border ice, which forms in areas of calm water, such as side channels. The signatures from freeze-over border ice and open-water, therefore, cannot be distinguished on this SAR image.

Juxtaposed ice cover and secondary consolidated ice cover

In Figure 5, the ice type varies from freeze-over border ice (A) to juxtaposed ice (B) and, then, to heavily consolidated ice (C). Tonal variations enable the classification of the two main ice types.

A consolidated ice cover predominantly occurs in river bends (C1, C2, C3, and C4). Between those zones lies a juxtaposed ice cover (B1, B2, and B3). At Location C1, an ice run caused secondary consolidation. The bright tone and the lobe-like shape of the consolidation run are in sharp contrast to the surrounding juxtaposed ice cover (B1) and freeze-over border ice (A1). The signature of secondary consolidated ice is very bright. Consolidated ice is composed of the same porous frazil slush as juxtaposed ice, but it is thicker than juxtaposed ice. Therefore, the volume scattering component from consolidated ice is assumed to be greater than from juxtaposed ice. The volume scattering from several layers of porous frazil slush and surface scattering at the very rough ice/water interface create a strong backscatter from consolidated ice.

Thermal break-up

On March 29, 2000 the ice front was located at Mile 234.5. The air temperature was approximately -2ºC and a thermal break-up was in progress.

In Figure 6, the ice front is clearly visible in the image (A). Brash ice is bridging the open water channel at two locations (B1 and B2). When consolidated, an ice cover of brash ice is thought to be characterized by a rough ice/water interface, which causes strong backscattering. Interestingly, brash ice at Location B1 appears brighter than brash ice at Location B2. This could have two reasons. Firstly, brash ice at Location B1 could have been more heavily consolidated than brash ice at Location B2. Secondly, the backwater directly upstream of the ice front could be flooding the ice surface at B2, thus reducing the diffuse scattering component and increasing the specular reflection component of the backscatter.

Flooded ice was identified at Location C. Although the tone of the flooded parts is the same as that of open water, the ice edge shows as a fine line thus making it possible to distinguish between open water and water on top of ice.

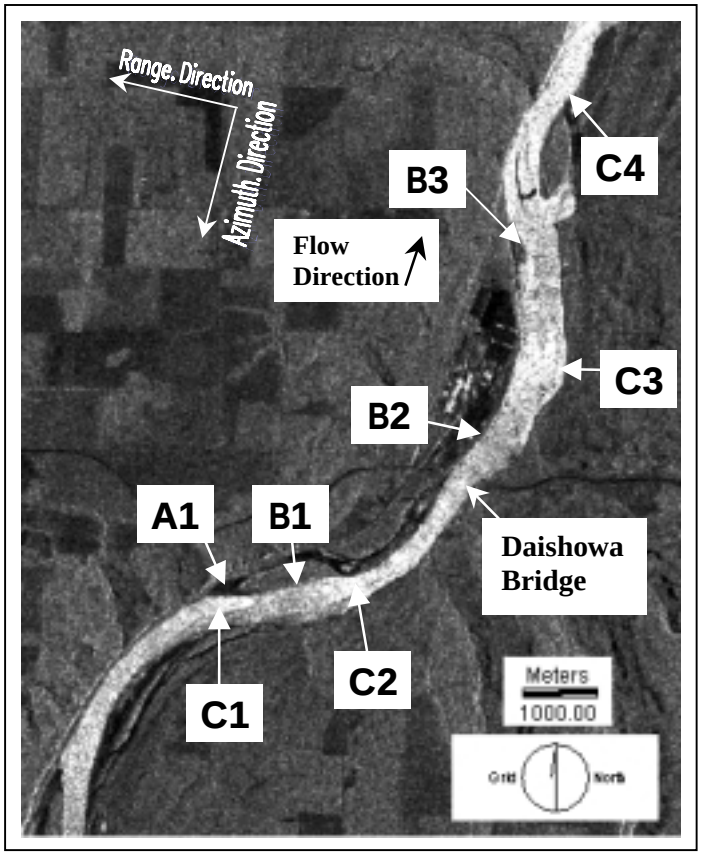

Figure 5: January 25, 2001 RADARSAT-1 image (F4N, descending)

Photographs taken on the day of image acquisition suggest that most of the ice cover in Figure 6 is water saturated (e.g. D). The wetting of the ice surface and the overlying snowpack is probably caused by flooding due to increased freshet flows and to a minor extent by snow-and icemelt. The radar return from these areas is relatively low. In some areas, free water is visible on top of the ice (E), as indicated by a very dark tone. Even a thin film of water on top of the ice surface will absorb and specularly reflect the radar energy, and, thus, cause low radar returns. However, the tone is not as dark as for open water.

In some isolated areas, ice features appear relatively bright (F). From analyzing photographs and topographic maps it was concluded that the ice and/or snow surface in these areas is slightly higher than the surrounding water level. This is due to the topographic relief or a large ice thickness. Therefore, the water table on top of a solid ice layer did not reach the ice and / or snow surface. It is proposed that large snow and ice grains and a rough ice / air or snow / air interface are responsible for the relatively strong radar return.

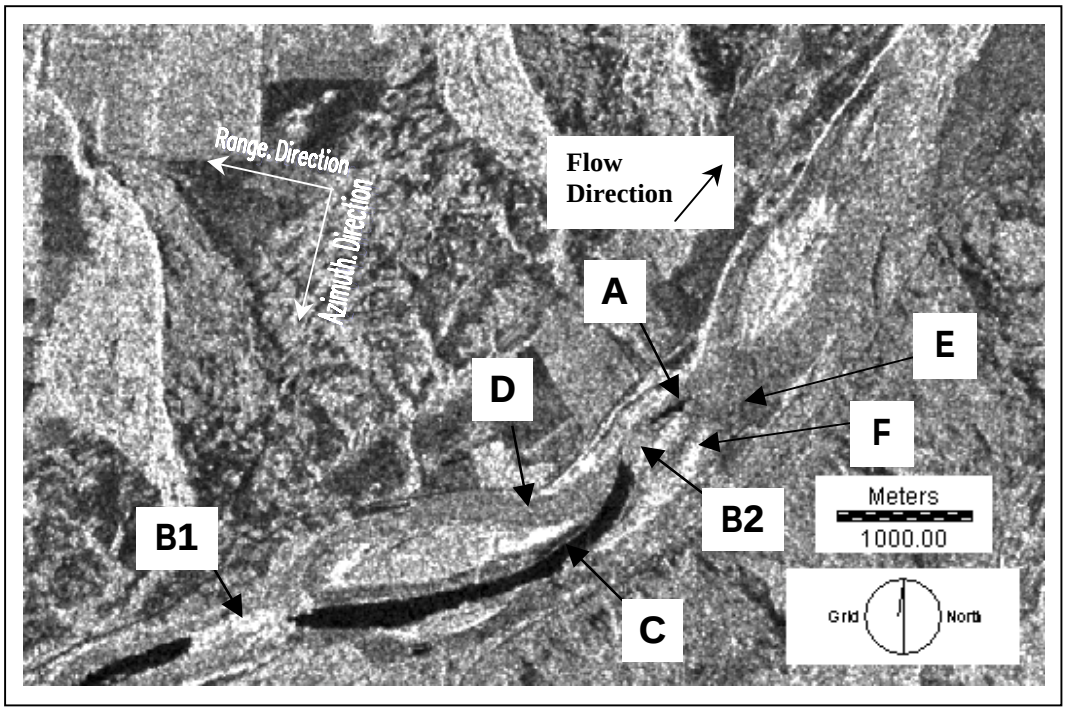

Figure 6: March 29, 2000 RADARSAT-1 image (F1F, descending)

Unsupervised Classification

Figures 7a, 7b, 7c and 8a, 8b, 8c, 8d compare the results from the Unsupervised Classification for the February 10, 2000 image with the SAR image and photos. In the automatically classified maps, four ice feature classes are used (Figure 7a and 8a).

In Figure 7a, the ice front is characterized by the transition from predominantly blue/cyan to cyan/yellow colors. As seen on the SAR image the ice front corresponds to the transition from frazil pans, frazil floes, and open water to a juxtaposed ice cover (Figure 7b). The photograph in Figure 7c shows the percentage ice coverage downstream of the gravel bar located in the center of the SAR image approximately 4.5 hours after image acquisition. The ice coverage as shown by the classification map and the original image corresponds well with the ice coverage as seen from the aircraft.

Immediately downstream of the ice front, the ice cover is composed of juxtaposed ice as indicated by areas of cyan/yellow colors on the classification map. The ice cover gradually consolidates in a downstream direction. The classification map shows an approximately equal percentage of red and orange colors for the consolidated ice cover. In the SAR image, increasing consolidation corresponds to an increasing brightness of the ice cover.

Figures 8a and 8b show the classification map and the original SAR image for the Peace River at Mile 175. This reach is characterized by consolidated ice at the upstream and downstream ends. At the upstream end of the image, a consolidation lobe can be identified in the SAR image by its bright tone and round terminus (Figure 8b). This consolidation lobe corresponds to predominantly red areas on the classification map (Figure 8a). Consolidated ice that resisted the shear forces can also be identified along the riverbanks by its bright tone in the SAR image. Figure 8c shows a close-up of the ice cover in the river bend. Consolidated ice and a smooth ice surface can be distinguished on the right and left side of the photograph, respectively. At the downstream end of the reach shown, consolidated ice appears in red on the classification map and in bright tones on the SAR image.

As a result of the consolidation, open-water areas opened up in the center of the reach, which appear in blue on the classification map and dark tone in the SAR image. Even the relatively narrow crack in the ice, shown in Figure 8d, can be identified in both the classification map and the SAR image. Remnants from the juxtaposition ice cover in the center of the reach and, possibly, new frazil ice accumulations compose the ice cover, as indicated by gray colors in the center of the reach in the SAR image and the predominantly cyan and yellow colors on the classification map.

It is important to recognize that the categories of this Unsupervised Classification do not provide the distribution of ice types. Instead, the categories provide the distribution of ice features with certain structural characteristics. The categories range from open water with a weak backscatter to ice with a strong backscatter. A strong backscatter corresponds to ice with a rough ice/water interface and a coarse ice structure. Ice features with a weak backscatter reflect a large part of the incoming microwaves specularly away from the imaging sensor and correspond to ice with a homogeneous structure and a smooth ice/water interface. The analyst can derive ice types from the classification using the proportion of ice features in an area as indicated by the colors in Figures 7a and 8a. For example, areas with predominantly red colors typically represent a heavily consolidated ice cover. Moderate ice consolidation is expected in areas characterized by a mix of yellow and red. A mixture of cyan and yellow is indicative of areas of juxtaposed ice. The percentage of cyan in areas of cyan and blue can be interpreted as the percentage of frazil pans and floes.

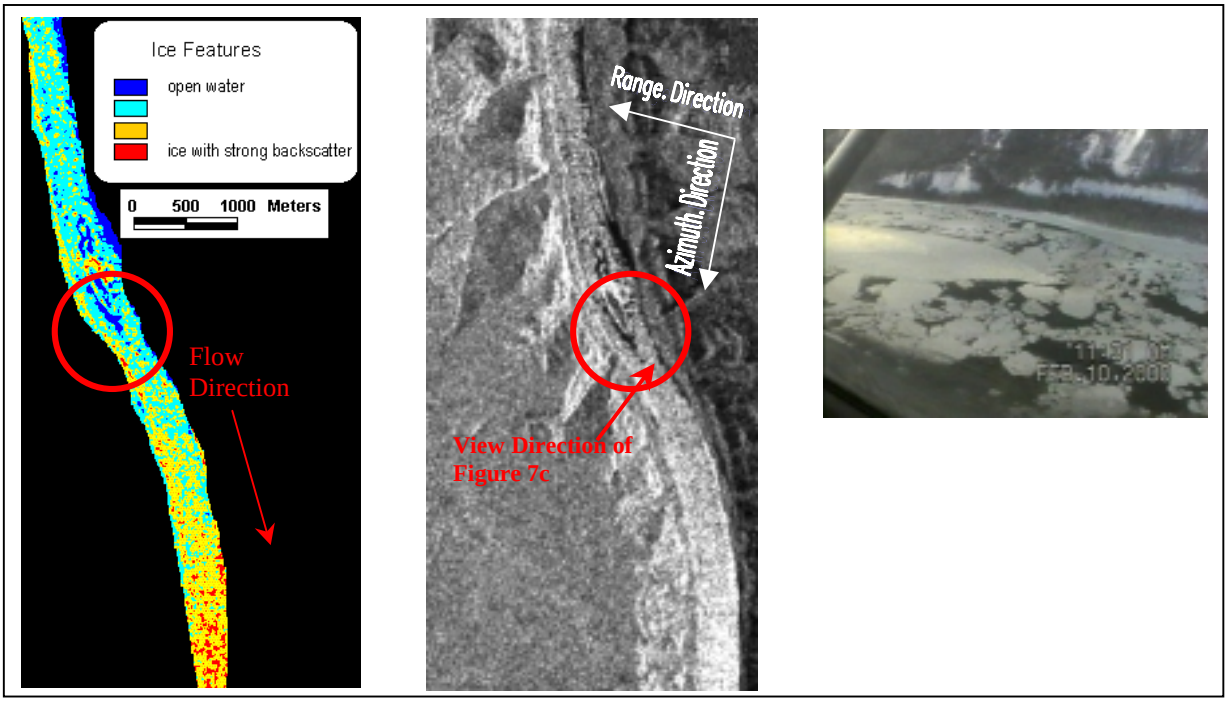

Figure 7a: February 10, 2000 – Unsupervised Classification

Figure 7b: February 10, 2000 – RADARSAT-1 Fine Beam image

Figure 7c: February 10, 2000 – Frazil pans and floes directly upstream of the ice front

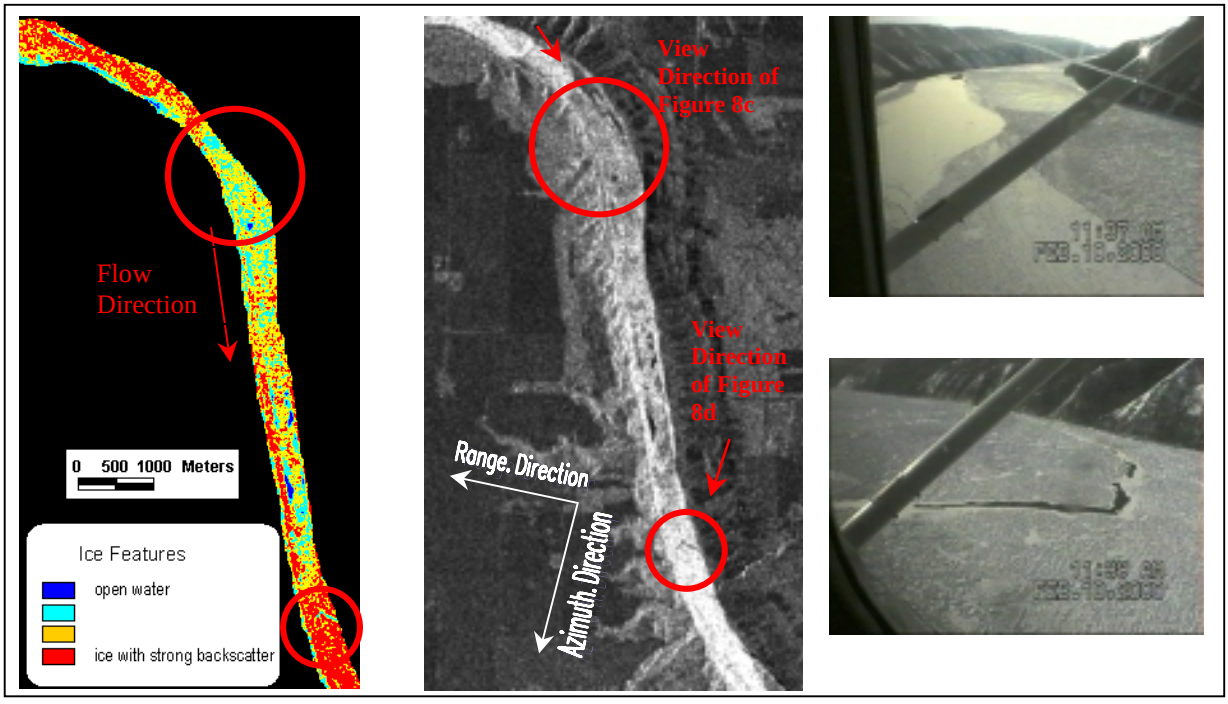

Figure 8a: February 10, 2000 – Unsupervised Classification

Figure 8b: February 10, 2000 – RADARSAT-1 Fine Beam image

Figure 8c: February 10, 2000 – Consolidated ice, juxtaposed ice

Figure 8d: February 10, 2000 – open water

Figures 7a, 7b, 7c and 8a, 8b, 8c, 8d show, that the spatial distribution of ice features on the classification maps very closely matches visible ice types. Areas of frazil pans and floes, the ice front, juxtaposed ice, consolidated ice, and open water coincide on the classification maps and the SAR images.

5. Summary and Conclusion

RADARSAT-1 SAR Fine Beam images acquired over the Peace River were examined for river ice types. The images were analyzed visually and using an Unsupervised Classification. The results were verified with video footage and photographs taken from a small aircraft.

By visually analyzing the images, the spatial distribution of frazil pans, frazil floes, juxtaposed ice, secondary consolidated ice, shore ice composed of frazil slush, melting ice, and brash ice was determined. It is assumed that the moderately rough ice/water interface and porous structure of frazil pans create the moderate to strong backscatter, which characterizes ice types formed from frazil slush. Frazil floes, frazil pans, juxtaposed ice, and shore ice composed of frazil slush can be distinguished by shape and location on the river. As frazil ice generation is the dominant river ice formation process in the Peace River, the transition from a partial to a complete ice cover is clearly visible on freeze-up images. Under certain freeze-up conditions, the head of the complete ice cover may differ by several hundreds of meters from the ice front, because parts of the complete ice cover may still be in motion. In this case, the location of the ice front may only be approximated from single SAR images. However, under most conditions encountered in this study, the location of the ice front matches the head of the complete ice cover, and was, therefore, discernible from the SAR images. Consolidated ice typically appears relatively bright, probably due to surface scattering from a very rough ice/water interface and volume scattering from several layers of frozen porous frazil slush. In particular, consolidation lobes contrast surrounding juxtaposed ice due to their shape and brightness. Ambiguities in the visual ice type analysis arise from open water and freeze-over border ice. It is assumed that freeze-over border ice specularly reflects microwaves at a smooth ice/water interface. As a result, radar returns from freeze-over border ice are relatively low and can be confused with open water. Melting ice appears relatively dark due to water partially covering the ice and specularly reflecting the microwave signals.

The four categories of an Unsupervised Fuzzy K-means Classification provide the distribution of ice features with certain structural characteristics. Final classification results show very promising outcomes, with a spatial distribution of ice features that matches very closely the visible ice types on the river.

When using SAR imagery operationally for river ice monitoring, several factors need to be considered. To utilize the 8 meter ground resolution of Fine Beam RADARSAT-1 images and still be able to capture the ice front, image scheduling depends heavily on ice observer information on the ice front location. The lead time for image orders was 48 hours. Forecasting the location of the ice-front at the time of the planned image acquisition is, therefore, critical. This is particularly true for East-West lying river reaches, which are perpendicular to the azimuth direction. Costs are limiting the operational use of RADARSAT-1 data. The price for a single Fine-Beam Path-Image is $CDN 4050. The additional costs for Priority Programming, that allows placing requests up to 3 days before the date of acquisition, and Near-Real Time Processing are $CDN 675 and $CDN 1350, respectively. In contrast, an ice observation flight costs approximately $CDN 2000 including labour costs. A major benefit of SAR images as a tool for river ice monitoring is their high information content. More time is available for the remote sensing analyst to identify ice types than for the ice observer in an aircraft. Furthermore, ice features can be exactly pinpointed on SAR images. In the Peace River region, images can be acquired approximately every 3 days. The coverage proved

to be sufficiently frequent for BC Hydro's needs. Of great benefit for a reliable image acquisition are the all-weather, day-and-night imaging capabilities of SAR sensors.

Building on the experience gained in this project, future work should continue on increasing the operational aspect of river ice monitoring with SAR images. The intent is to automate as many tasks as possible, reducing user input and the time required to produce a final product. In particular, future work should focus on the automated extraction of a thematic layer, which identifies river ice types. Consequently, more field data is required to translate ice type information into ice strength information.

6. Acknowledgements

The authors would like to thank E. Weiss, F. Rau, and M. Braun for their valuable comments on the manuscript.

7. References

Andres, D., 1995. Frazil Generation and Ice Floe Formation on a Regulated River. Proc. 8th Workshop on the Hydraulics of the Ice Covered Rivers, Kamloops, BC, 57-76.

Assaf, H., Parmely, L., Chan-McLeod, A., and Galvagno, P., 1995. An Analysis of Events Leading to the February 1992 Flooding of the Town of Peace River, Alberta. Proc. 8th Workshop on the Hydraulics of the Ice Covered Rivers, Kamloops, BC,1-42.

Bryan, M.L. and Larson, R.W., 1975. The Study of Freshwater Lake Ice using Multiplexed Imaging Radar. Journal of Glaciology, Vol.14 (72), 445-457.

Cooper, D.W., Mueller, R.A., and Schertler, R.J., 1976. Remote Profiling of Lake Ice using an S-band Short-Pulse Radar aboard an All-Terrain Vehicle. Radio Science11, 375-381.

Drinkwater, M.R., 1989. Limex '87 Ice Surface Characteristics: Implications for C-Band SAR Backscatter Signatures. IEE Transactions on Geoscience and Remote Sensing, Vol. 27, No.5, 501-513.

Elachi, C., Bryan, M.L. and Weeks, W.F., 1976. Imaging Radar Observations of Frozen Arctic Lakes. Remote Sensing of Environment, Vol.5, 169-175.

Evans,S., 1965. The Dielectric Properties of Ice and Snow – A Review. Journal of Glaciology, 5, 773-792.

Hall, D., 1998. Remote Sensing of Snow and Ice Using Imaging Radar In: Henderson and Lewis (ed.), Principles and Applications of Imaging Radar - Manual of Remote Sensing, 3rd Edition, Vol.2, John Wiley and Sons, 677-703.

Hallikainen, M. and Ullaby, F.T., 1986. Dielectric and Scattering Behavior of Snow at Microwave Frequencies. Proc. of the International Geoscience and Remote Sensing Symposium, Zurich, Switzerland, 87-91.

Hallikainen, M. and Winebrenner, D.P., 1992. The Physical Basis for Sea Ice Remote Sensing. In: Carsey (ed.), Microwave Remote Sensing of Sea Ice, Geophysical Monograph 68, American Geophysical Union, 29-46.

Leconte, R. and Klassen, P.D., 1991. Lake and River Ice Investigations in Northern Manitoba Using Airborne SAR Imagery. Arctic, Vol.44, Supp.1, 153-163.

Morris, K.M., Jeffries, M.O., and Weeks, W.F., 1995. Ice Processes and Growth History on Arctic and Subarctic Lakes using ERS-1 SAR data. Polar Record, Vol.31(177), 115-128.

RADARSAT International, 1999. RADARSAT Illuminated: Your Guide to Products and Services. http://www.rsi.ca/classroom/RSIUG98(499).pdf.

Raney, K.R., 1998. Radar Fundamentals: Technical Perspective. In: Henderson and Lewis (ed.), Principles and Applications of Imaging Radar - Manual of Remote Sensing, 3rd Edition, Vol.2, John Wiley and Sons, 9-130.

Rau, F., Brau, M., Saurer, H., Gossmann, H., Kothe, G., Weber, F., Ebel, M., and Beppler, D., 2000. Monitoring Multi-Year Snow Cover Dynamics on the Antarctic Peninsula Using SAR Imagery. Polarforschung 67 (1/2), 27-40.

Shen, H.T., 1996. River Ice Processes – State of Research. 13th International Symposium on Ice. Bejing, China, 825-833.

Trillium Engineering and Hydrographics Inc, Northwest Hydraulic Consultants Ltd., and Thurber Engineering Ltd., 1996. Ice Formation and Breakup at the Town of Peace River – A study of Regulated Conditions. Edmonton, Alberta, 1969-94.